Spadaccini (1989) because the relevant extinction corrections were determined from F_o *versus* F_c agreement. The positive charge on the transition metals would be correspondingly underestimated in that review, changing slightly the trends originally reported by these authors.

$\Delta\rho$ maps for the 0.7 Å data shown in Figs. 1 and 2 are (100) and (110) planes corresponding to Figs. 1(*a*) and 2 of Buttner & Maslen (1992). Although the maps for the different radiations are similar in general, there are differences in detail. At the atomic sites local maxima in the synchrotron radiation map replace minima in the Mo $K\alpha$ map.

The region of depleted density surrounding the Sr and Ti cations is clearly defined in Figs. 1 and 2. There is also a strong minimum in the density at the structural cavity (relative to the rock-salt structure) mid-way between adjacent Sr atoms. Electron density is transferred from the vicinity of the atoms and the structural cavity to the broad sea of positive density in the internuclear region.

To within a scale factor $\Delta\rho$ near the Ti position closely resembles that observed near Zn in the isostructural $KZnF_3$ compound, as reported using similar data measured at the Photon Factory (Maslen, Spadaccini, Ito, Marumo & Satow, 1995). In both maps there is a local maximum in $\Delta\rho$ at the transition-metal atom sites, flanked by minima directed towards the K or Sr cations. There are local maxima 0.8 and 1.0 Å along Sr—Ti and K—Zn, respectively. These features near Ti are less compact than those near Zn, as would be expected since the effective nuclear charge for Ti is lower than that for Zn. Ti^{4+} and Zn^{2+} are closed-shell cations with outer shell configurations $3d^0$ and $3d^{10}$, respectively. The higher degree of polarization around Ti is consistent with a formally empty $3d^0$ subshell being more polarizable than a $3d^{10}$ configuration. Presumably, that subshell is partly occupied because of overlap with the valence electrons from neighbouring O and Sr atoms.

The contributions of computer programs by their authors R. Alden, G. Davenport, R. Doherty, W. Dreissig, H. D. Flack, S. R. Hall, J. R. Holden, A. Imerito, R. Merom, R. Olthof-Hazekamp, M. A. Spackman, N. Spadaccini & J. M. Stewart to the *Xtal*3.0 system (Hall & Stewart, 1990), used extensively in this work, is gratefully acknowledged. Thanks are also due to D. C. Creagh, who calculated the dispersion corrections. This research was supported by the Australian Research Council.

References

ALCOCK, N. W. (1974). *Acta Cryst.* A**30**, 332–335.
BACHMAN, R., KOHLER, H., SCHULZ, H. & WEBER, H.-P. (1985). *Acta Cryst.* A**41**, 35–40.
BUTTNER, R. H. & MASLEN, E. N. (1992). *Acta Cryst.* B**48**, 639–644.
CREAGH, D. C. (1990). Private communication.
HALL, S. R. & STEWART, J. M. (1990). Editors. *Xtal*3.0 *Reference Manual*. Univs. of Western Australia, Australia, and Maryland, USA.
HIRSHFELD, F. H. (1977). *Isr. J. Chem.* **16**, 198–201.
MASLEN, E. N. & SPADACCINI, N. (1989). *Acta Cryst.* B**45**, 45–52.
MASLEN, E. N. & SPADACCINI, N. (1993). *Acta Cryst.* A**49**, 661–667.
MASLEN, E. N., SPADACCINI, N., ITO, T., MARUMO, F. & SATOW, Y. (1995). Submitted for publication.
REES, B. (1977). *Isr. J. Chem.* **16**, 180–186.
SATOW, Y. & IITAKA, Y. (1989). *Rev. Sci. Instrum.* **60**, 2390–2393.
ZACHARIASEN, W. H. (1967). *Acta Cryst.* A**23**, 558–564.

Acta Cryst. (1995). B**51**, 942–951

The Chemical Bond and Atomic Displacements in $SrTiO_3$ From X-ray Diffraction Analysis

BY YU. A. ABRAMOV AND V. G. TSIRELSON

Mendeleev University of Chemical Technology, Moscow 125047, *Russia*

V. E. ZAVODNIK AND S. A. IVANOV

Karpov Institute of Physical Chemistry, ul.Obucha 10, *Moscow* 103064, *Russia*

AND I. D. BROWN

Institute for Material Research, McMaster University, Hamilton, Ontario, Canada L8S 4M1

(*Received* 27 *December* 1994; *accepted* 15 *March* 1995)

Abstract

The deformation electron-density (dynamic Fourier) maps and the anharmonicity of atomic displacements in strontium titanate, $SrTiO_3$ (Gram–Charlier model), were studied by high-precision single-crystal X-ray diffraction analysis at 145(1) and 296(2) K. Space group $Pm\bar{3}m$, cubic, $\lambda(\text{Mo } K\alpha) = 0.71069$ Å, $Z = 1$, $F(000) = 84$,

©1995 International Union of Crystallography
Printed in Great Britain – all rights reserved

$T = 145(1)$ K, $a = 3.8996(5)$ Å, $V = 59.30(2)$ Å^3, $D_x = 5.138(2)$ g cm^{-3}, $\mu = 26.728$ mm^{-1}, $R = 0.0063$, $wR = 0.0040$, $S = 1.05$ for 131 unique reflections and $T = 296(2)$ K, $a = 3.901(1)$ Å, $V = 59.36(5)$ Å^3, $D_x = 5.133(4)$ g cm^{-3}, $\mu = 26.700$ mm^{-1}, $R = 0.0071$, $wR = 0.0050$, $S = 1.40$ for 109 unique reflections. Strong anharmonicity of the atomic displacements was observed for all atoms at 145 K and for Ti and O atoms at 296 K. These are explained by a model in which electronic instability in the TiO_6 octahedron leads to a displacement of the Ti atom from the center of the octahedron, and the lattice instability resulting from the consequent stretching of the Sr—O bonds leads to a rotation of the octahedra. Both distortions show only short-range order at the temperatures studied, but show indications of freezing out as the temperature is lowered towards the rotational phase transition at 106 K. The experimental dynamic Fourier deformation electron-density maps and the Hirshfeld atomic charges were calculated.

Introduction

Most ABO_3 perovskite compounds show one of two types of distortion from the parent cubic structure as the temperature is lowered, either the B atom moves off-center in its octahedron to give a ferroelectric phase, or the BO_6 octahedra rotate to reduce the number of O atoms bonding to A. The first distortion occurs in compounds where A is large compared with B, *e.g.* $BaTiO_3$, the second is found in compounds where A is small compared with B, *e.g.* $CaTiO_3$.

The influence of cation size on the distortion can be interpreted in terms of the bond valence model (Brown, 1991, 1992). In this model, the bond between atoms i and j is assigned a valence s_{ij} which has the property that the sum of all the bond valences received by atom i is equal to its atomic valence V_i (formal oxidation state), as given by (1)

$$\sum_j s_{ij} = V_i. \qquad (1)$$

Equation (1), together with (2) which has the effect of ensuring a uniform distribution of valence between the bonds, allows one to predict unique values for the bond valences in any given network of bonds

$$\sum_{\text{loop}} s_{ij} = 0. \qquad (2)$$

An important property of the bond valence is that it correlates with the bond length R_{ij} according to (3)

$$s_{ij} = \exp[(R_o - R_{ij})B], \qquad (3)$$

where R_o and B are empirical constants which have been tabulated for most common bond types (Brown & Altermatt, 1985). With these three equations it is possible to predict the length of the bonds in perovskites and hence to take into account the relative sizes of the atoms.

In the cubic perovskite phase all 12 A—O bonds are equivalent, as are all six B—O bonds, so the bond valences are $s_{AO} = V_A/12$ and $s_{BO} = V_B/6$. Substituting these values for a particular compound into (3) yields the lengths that would be expected for the A—O and B—O bonds. Thus, for $BaTiO_3$ the length of the Ba—O bonds is predicted to be 2.95 Å and the length of the Ti—O bond 1.96 Å. In ideal crystals, the ratio of these lengths is constrained by geometry to be $2^{1/2}$ since each bond length is related to the lattice parameter a by

$$a = 2^{1/2}R_{AO} = 2R_{BO}. \qquad (4)$$

In general, the ratio of the predicted values of R_{AO} and R_{BO} will not be $2^{1/2}$: in $BaTiO_3$, for example, this ratio is 1.50 rather than 1.41, so that, in cubic $BaTiO_3$ the Ti—O bond must be stretched and the Ba—O bond compressed. The type and size of the strain expected in a cubic perovskite is related to the tolerance factor given by the ratio $a(A)/a(B)$, where $a(A)$ is the lattice parameter calculated from the predicted value of R_{AO} and $a(B)$ is the lattice parameter calculated from the predicted value of R_{BO}. Only if this ratio is exactly 1.0 will the bonds show no strain. For larger ratios the B—O bond is stretched, for smaller ratios the A—O bond is stretched.

It follows from the form of (3) that any atom whose bonds are stretched will be stabilized by distorting the environment of the atom in a way that changes the individual bond lengths without changing their average (the Distortion Theorem given by Brown, 1992). If $a(A)/a(B)$ is greater than 1, a distortion is expected in which the B atom moves off-center in its octahedron (displacive distortion), leading to the ferroelectric phases found in $BaTiO_3$ [$a(A)/a(B) = 1.06$]. If $a(A)/a(B)$ is less than 1, the octahedra twist in such a way as to make some of the A—O bonds longer and some shorter (rotational distortion), as found in $CaTiO_3$ [$a(A)/a(B) = 0.95$]. Most ABO_3 compounds which crystallize with the perovskite structure show one or other of these distortions at room temperature; only at high temperatures, if at all, do they adopt the parent cubic structure.

$SrTiO_3$ occupies a special position in this series because the Sr and Ti atoms are exactly matched, *i.e.* $a(A)/a(B) = 1.00$. Consequently, $SrTiO_3$ has the undistorted cubic structure at room temperature, although below 106 K it undergoes a rotational transition to a tetragonal ($I4/mcm$) phase (Unoki & Sakudo, 1967) and at still lower temperatures transforms to other less well characterized phases (Lytle, 1964). Since it is cubic at room temperature, $SrTiO_3$ is a good compound to use to investigate the behavior of the structure as it cools down to the phase transition.

The mechanism of the phase transformation in perovskites is often described in terms of the phonon model (Stirling, 1972; Bruce & Cowley, 1981), which assumes that the atoms move in harmonic potential wells.

Although the phonon frequencies should not depend on temperature, the instability of the cubic structure connected with the bond strain causes a lowering of the renormalized (quasiharmonic) frequency of one of the phonons with temperature, reaching zero at the transition point (soft mode concept). At this point the corresponding mode freezes out at the extreme position given by its eigenvalue (Glazer, 1972) and a phase transition occurs. The anharmonic contribution to the soft mode, which is responsible for the nature of this transition, is determined by peculiarities of atomic potential wells, as discussed below.

In order to reveal the deviation of the atomic potential wells from harmonicity, anharmonic atomic displacement parameters must be introduced into any structural model refined using the diffraction data. Neutron diffraction gives the average positions and mean atomic displacements of the atomic nuclei and is thus particularly suitable for measuring the nuclear probability distribution functions (PDF's). X-rays and γ-rays are diffracted by the electrons, and so can be used to determine the space and time-averaged electron density (ED), which is the convolution of the nuclear PDF's with the instantaneous electron density of the local structure. The model approach allows these two effects to be approximately separated, so that the atomic PDF's reconstructed from results of high-angle refinement can be used to examine the anharmonic motion of the atoms and the observed electron density can be compared with the thermally smeared electron density obtained from quantum mechanical calculations.

The role of covalent bonding in properties of perovskites has been pointed out by Megaw (1952). Later first-principle calculations on the ideal cubic structure of $SrTiO_3$ by Weyrich & Siems (1985), Weyrich & Madenach (1990) and Xu, Ching & French (1990) have shown that the Sr—O bond has predominantly ionic character, but that there is an important covalent contribution to the Ti—O bond. The experimental electron-density distribution of $SrTiO_3$ in the cubic phase has been measured by Buttner & Maslen (1992). Unfortunately, their seven sets of diffraction intensities measured at 298 K from five very small irregularly shaped samples show a significant range of atomic charges and variations in the deformation electron-density maps, probably due to severe extinction in some samples. However, all their maps show a significant concentration of the density in the Ti—O bond. Palmer (1993), using γ-rays, found an electron-density concentration in the Sr—O bond but not in the Ti—O bond.

The principal cause of the anharmonicity in perovskites is the size effect noted above, but a secondary cause arises from the overlap that can occur between the vacant d orbitals of a transition metal ion (*e.g.* Ti^{4+}) and the filled p orbitals of its O^{2-} ligands, that is to say, from the covalent contribution to the Ti—O bond. The effect is well attested (Kunz & Brown, 1995) and can be described either as a second-order Jahn–Teller distortion (Burdett, 1980) or a dynamic covalency (Bilz, Buettner, Bussmann-Holder & Vogl, 1987). Allowing the B atom to move from the center of its octahedron may result in a d–p interaction, which lowers the electronic energy of the crystal. The effect has been reproduced in quantum mechanical calculations (Weyrich & Siems, 1985; Weyrich & Madenach, 1990; Cohen & Krakauer, 1990) for particular configurations, although calculations are usually only performed for the atoms in their high-symmetry locations (Xu, Ching & French, 1990).

An anisotropy in the oxygen displacement in cubic $SrTiO_3$ has been observed by Hutton & Nelmes (1981) with neutron diffraction at 111 K ($= T_c + 5$ K), by Palmer (1993) with γ-rays at 298 and 111 K, and by Buttner & Maslen (1992) with X-ray diffraction at 298 K. Palmer also found significant anharmonicity in the Ti and Sr atomic displacements at room temperature, but no anharmonicity was detected by either Palmer (1993) or Hutton & Nelmes (1981) at 111 K.

While previous workers all agree on the anisotropy of the O-atom motion corresponding to the libration of the TiO_6 octahedra, the expected precursor to the rotational phase transition observed at 106 K, they disagree on the nature of the Ti—O and Sr—O bonding and the presence of anharmonicity in the cation motions. The present study is an attempt to clarify the problem and to develop an anharmonic electron-dynamical model of the $SrTiO_3$ crystal using high-precision X-ray diffraction measurements at 296 and 145 K.

Experimental

Pure colorless transparent $SrTiO_3$ single crystals were prepared for X-ray diffraction investigations. The crystals were grown by the Verneuil method and tested by surface X-ray emission spectral analysis and dielectric measurements (Ivanov, Belokopytov, Buzin, Sychev & Chuprakov, 1978). The crystals, which initially had irregular shapes, were ground in a compressed-air mill yielding samples of almost perfect spherical shape. After preliminary studies, a crystal with radius 0.06 mm was chosen for the accurate X-ray analysis since good reflection profiles were observed with this sample.

The measurements at 296 (2) and 145 (1) K were obtained on a Syntex $P\bar{1}$ diffractometer with β-filtered (Nb) Mo $K\alpha$ radiation. Total intensity profiles of reflections were recorded. A ψ-scan was used for low-angle reflections in order to avoid the distortion of the intensities by multiple scattering. Three standard reflections in three orthogonal directions measured every 100 reflections were stable within the range $\pm 1\%$. Integrated intensities were calculated using the Streltsov & Zavodnik (1989) profile analysis method and analytically corrected for Lorentz, polarization and absorption factors. Experimental correction for thermal diffuse

Table 1. *Crystal, experimental and refinement data for* $SrTiO_3$

	Data set no. (I)	(II)
Temperature (K)	145 (1)	296 (2)
Space group	$Pm\bar{3}m$	$Pm\bar{3}m$
a (Å)	3.8996 (5)	3.901 (1)
V (Å^3)	59.30 (2)	59.36 (5)
D_x (g cm^{-3})	5.138 (2)	5.133 (4)
μ for Mo $K\alpha$ (mm^{-1})	26.728	26.700
Radius of specimen (mm)	0.06	0.06
Radiation	Mo $K\alpha$	Mo $K\alpha$
Wavelength (Å)	0.71069	0.71069
Monochromator	None	None
Diffractometer	Syntex $P\bar{1}$	Syntex $P\bar{1}$
$2\theta_{max}$ (°)	124.13	139.38
$(\sin\theta/\lambda)_{max}$ (Å^{-1})	1.243	1.320
Scan mode	ω–2θ	ω–2θ
Initial scan width (°)	0.8	0.8
Scan speed (° min^{-1})	1–12	1–12
No. of reflections measured	1463	2015
No. of unique reflections	131	109
R_{int} (absorption corrected)	0.0227	0.047
Mode of refinement	$F(hkl) > 3\sigma(F)$	$F(hkl) > 3\sigma(F)$
Weighting scheme	$w = 1/[\sigma^2(F) + 0.0001F^2]$	
Extinction account formalism	Zachariasen (1967)	Zachariasen (1967)
TDS correction	Experimental (Zavodnik, Stash, Tsirelson & Feil, 1994)	Experimental (Zavodnik, Stash, Tsirelson & Feil, 1994)

Table 2. *Results of the high-order structural model refinements for* $SrTiO_3$

	Temperature 145 K (I)	145 K (II)	296 K (I)	296 K (II)
Model No.*				
y_{min} (*hkl*)	0.90 (200)	0.90 (200)	0.90 (200)	0.90 (200)
wR†	0.0040	0.0042	0.0050	0.0055
R†	0.0063	0.0066	0.0071	0.0073
S†	1.05	1.10	1.40	1.20
Sr				
U (Å^2)	0.00364 (3)	0.00366 (3)	0.00785 (3)	0.00789 (3)
$d_{1111} \times 10^4$	−0.00080 (17)	−0.00089 (17)	0‡	0‡
$d_{1122\times10^4}$	0‡	0‡	0‡	0‡
Ti				
U (Å^2)	0.00313 (6)	0.00313 (6)	0.00556 (8)	0.00558 (9)
$d_{111} \times 10^4$	−0.00086 (30)	−0.00083 (30)	−0.00232 (23)	−0.00236 (27)
$d_{1122} \times 10^4$	0‡	0‡	−0.00076 (10)	−0.00075 (11)
O				
x	1/2	1/2	1/2	1/2
U_{11} (Å^2)	0.00247 (26)	0.00211 (29)	0.00463 (35)	0.00472 (38)
U_{22} (Å^2)	0.00755 (13)	0.00677 (20)	0.01205 (13)	0.01110 (30)
$d_{1111} \times 10^4$	−0.00194 (95)	−0.00307 (99)	−0.00236 (101)	−0.00229 (112)
$d_{2222} \times 10^4$	0‡	−0.00205 (86)	0	−0.00229 (104)
$d_{1122} \times 10^4$	0‡	0‡	0‡	0‡
$d_{2233} \times 10^4$	0.00110 (54)	0‡	0‡	−0.00150 (64)

Temperature factor $T_j(\mathbf{h})^{GC} = T_j(\mathbf{h})^{har}\{1 + [(2\pi i)^3/3!]c_j^{pqr}h_p h_q h_r + [(2\pi i^4)/4!]d_j^{pqrs}h_p h_q h_r h_s\}$, where $T_j(\mathbf{h})^{har} = \exp[-2\pi^2 a^{*2}(h^2 U_{j11} + k^2 U_{j22} + l^2 U_{j33})]$.

* Models (I) and (II) correspond to refinement with atomic and ionic scattering factors, respectively.

† Results of high-order refinement ($\sin\theta/\lambda > 0.6$ Å^{-1}).

‡ The small and insignificant parameters were fixed to zero.

scattering according to Zavodnik, Stash, Tsirelson & Feil (1994) was applied. The corresponding TDS correction values did not exceed 1.5 and 5% at 145 and 296 K, respectively. Selected experimental data are given in Table 1.

Since the earlier theoretical (Weyrich & Siems, 1985; Weyrich & Madenach, 1990; Xu, Ching & French, 1990) and experimental (Buttner & Maslen, 1992) studies have revealed the deviation of the chemical bonding in $SrTiO_3$ from pure ionic, both ionic and atomic anharmonic structural models were independently used in the full-matrix least-squares refinement of the $SrTiO_3$ crystal. The corresponding scattering factors and anomalous scattering corrections were taken from *International Tables for Crystallography* (1992 Vol. C) and from Hovestreydt (1983) for O^{2-}. The anharmonicity of the atomic displacements was modeled using a Gram–Charlier expansion of the PDF up to tensors of fourth rank (*International Tables for Crystallography*, 1992, Vol. C). Preliminary studies showed that the isotropic secondary extinction corrections of both the Becker & Coppens (1974) and Zachariasen (1967) models result in the same deformation ED maps. Therefore, the simpler Zachariasen model was used. The secondary extinction in the crystal studied appeared not to be severe at both temperatures of the experiment. The minimum value of the isotropic extinction correction y was 0.9 for the (200) reflections.

Refinement was based on $|F|$ with least-squares weights equal to $1/[\sigma^2(F) + 0.0001F^2]$ at both temperatures. The scale factor and extinction parameter were determined using all reflections, while atomic displacement tensor elements were refined in the high-angle region [$\sin\theta/\lambda > 0.6$ Å^{-1} for O^{2-} (O) and $\sin\theta/\lambda > 0.75$ Å^{-1} for Sr^{2+} (Sr) and Ti^{4+} (Ti)]. After a few cycles of refinement, the small symmetry-allowed fourth-rank components of displacement tensors with values less than 2.0σ were fixed at zero and the refinement was continued. After this stage of refinement was completed, the anomalous scattering contribution was removed from the experimental structure factors according to de Titta, as quoted by Takazawa, Ohba & Saito (1988). The refinement was then repeated with the corrected structure factors and without the use of anomalous scattering factors. The final results were statistically correct according to the test of Abrahams & Keve (1971). The results of the refinement are given in Table 2.*

The program system *PROMETHEUS* (Zucker, Perenthaler, Kuhs, Bachman & Schulz, 1983) was used in all calculations.

Results and discussion

Electron densities and atomic charges

The results of both models of the high-order $SrTiO_3$ structure refinements using the measurements made at

* A list of structure factors and diagrams of standard deformation electron-density and difference maps have been deposited with the IUCr (Reference: SH0063). Copies may be obtained through The Managing Editor, International Union of Crystallography, 5 Abbey Square, Chester CH1 2HU, England.

145 K were used to calculate difference electron-density maps. The (100) and (011) planes of the standard deformation electron-density map ($\delta\rho$), *i.e.* the difference between observed electron density and that calculated from neutral spherical atoms (atomic model of refinement), and the $\delta\rho_{ion}$ map showing the difference between observed density and that calculated from free Sr^{2+}, Ti^{4+} and O^{2-} ions (ionic model of refinement) are shown in Figs. 1 and 2, respectively.

To estimate the precision of the difference maps, we calculated the $\sigma(\delta\rho)$ map according to Lobanov, Tsirelson & Shchedrin (1990), taking into account the experimental uncertainties in the scale factor and displacement parameters. The estimated standard deviation values of 4.60, 2.52 and 0.40 e Å^{-3} were found on this map at the sites of the Sr, Ti and O atoms, respectively. In the internuclear regions, which are the regions of greatest interest, $\sigma(\delta\rho)$ was less than 0.07 e Å^{-3}, *i.e.* the uncertainty is less than the 0.1 e Å^{-3} contour interval in Figs. 1 and 2. Thus, the values of $\delta\rho$ close to the atom sites should be ignored, but the details shown in the figures in the internuclear region are all statistically significant.

The largest significant feature in the $\delta\rho$ map is a peak of 0.39 e Å^{-3} observed along the Ti—O bonds 0.62 Å

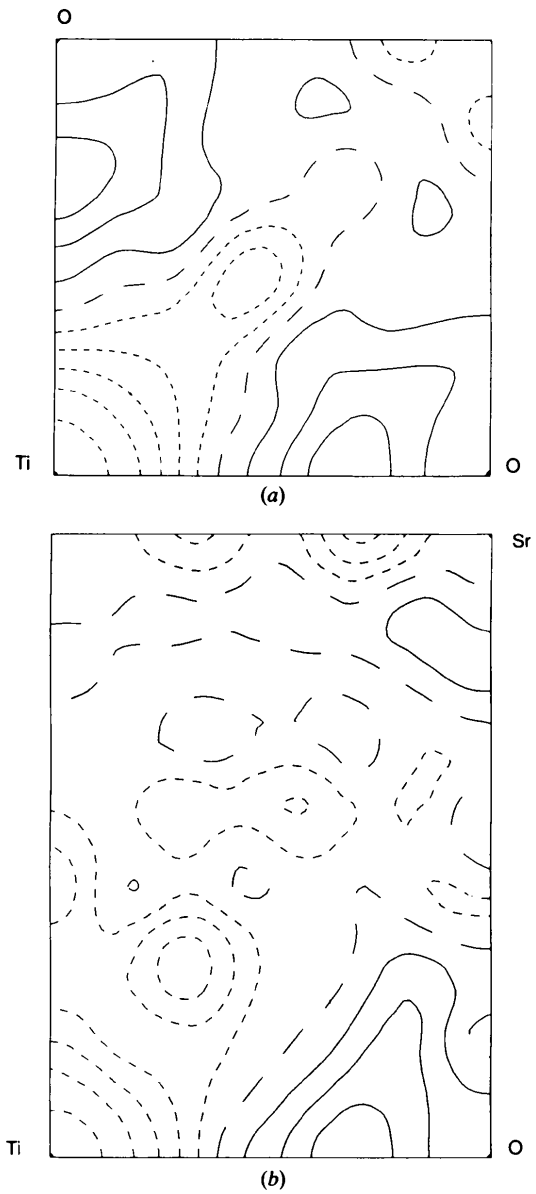

Fig. 1. Standard deformation electron-density maps $\delta\rho(\rho - \rho_{atom})$ for $SrTi_3$: sections in (100)-*a* and (011)-*b* planes. Contour intervals are 0.1 e Å^{-3}. Positive, zero and negative contours are represented by solid, long and short dashed lines, respectively.

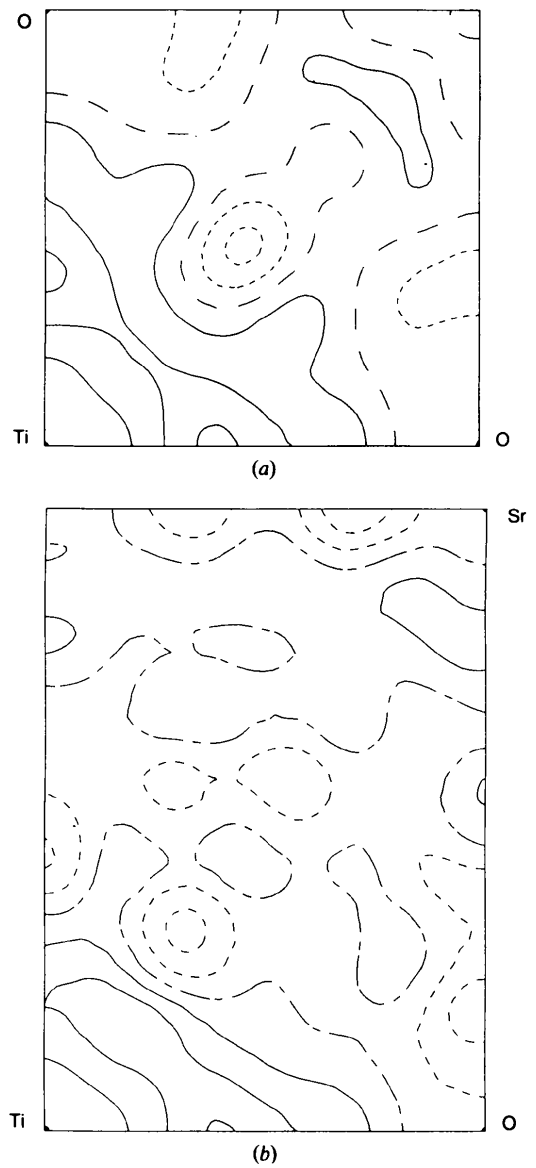

Fig. 2. Difference $\delta\rho_{ion}$ $(\rho - \rho_{ion})$ maps for $SrTiO_3$: sections in (100)-*a* and (011)-*b* planes. Contouring as in Fig. 1.

from the O-atom position (Figs. 1*a* and *b*). A similar though smaller peak (0.15 e Å^{-3}) is found 0.57 Å from Sr along the Sr—O bonds. Negative peaks (−0.34 e Å^{-3}) are found at the same distance from Sr and at 1.2 Å from Ti (Fig. 1*a*) in the regions between the metal–oxygen bonds. The $\delta\rho_{ion}$ map differs in a predictable way from the $\delta\rho$ map (Fig. 2*a*): the large peak of excess density in the Ti—O bond is shifted closer to the Ti^{4+} ion. At the same time, the electron density around the Sr^{2+} ion remains qualitatively the same. The atomic charges, evaluated numerically using the Hirshfeld (1977) method, are Ti +0.84, Sr +0.51 and O −0.45 e.

The character of the chemical bond between Ti and O is particularly interesting in $SrTiO_3$, because the states near the Fermi level are associated with the relative contributions of the 3*d* orbitals of Ti and 2*p* orbitals of O (Weyrich & Madenach, 1990; Xu, Ching & French, 1990). It is these states which are responsible for the electronic properties of $SrTiO_3$, including the electronic instability which, as shown by Bilz, Buettner, Bussmann-Holder & Vogl (1987), occurs through a lowering of the energy of the nonbonding 2*p* O orbitals as the Ti atom displacement mixes in contributions from the metal.

The experimental difference electron-density distributions as well as estimated atomic charges cannot give a precise picture of the nature of the chemical bonding between atoms in $SrTiO_3$, because they retain the cubic symmetry of the crystal and do not reflect the true distorted nature of the TiO_6 octahedra (see below). Nevertheless, the $\delta\rho$ maps in the (100) plane (Fig. 1*a*) reflect the strong ionic contribution to the Ti—O interaction, since excess ED is shifted toward the O atom. At the same time, the charge of +0.84 e on the Ti ion and the excess $\delta\rho_{ion}$ density near the Ti position along the Ti—O line (Fig. 2*a*) are evidence for the partially covalent nature of the Ti—O *d–p* σ-bond. The positive density in the map near the Ti^{4+} ion in the [111] directions suggests some concentration of nonbonding Ti(3*d*)-electrons of *t*-symmetry (Fig. 2*b*). In the language of the ionic model we can say that a significant amount of charge is transferred from the O^{2-} ion back to the Ti^{4+} ion and consequently the real Ti and O ionic charges are less than the formal oxidation numbers of +4 and −2, respectively, in agreement with the values of the atomic charges given above.

The partial covalence of the Ti—O bond found agrees with the results of the LMTO (Weyrich & Siems, 1985) and LAPW (Cohen & Krakauer, 1990) calculations, which have shown that electron density, corresponding to a *d–p* σ-molecular orbital, is distributed between both atoms. There is also good qualitative correspondence between the experimental $\delta\rho_{ion}$ distribution in the Ti—O bond of $SrTiO_3$ and that calculated by Cohen & Krakauer (1990) for $BaTiO_3$.

The observed covalence contribution to the Ti—O interaction is favorable to the TiO_6 octahedron electronic instability in $SrTiO_3$ and can be one of the sources of the anharmonicity in this compound (Kunz & Brown, 1995).

The $\delta\rho$ and $\delta\rho_{ion}$ distributions along the Sr—O bond (Figs. 1*b* and 2*b*) have revealed an anisotropy of electron density around the Sr nucleus. Such behavior can be expected if the asphericity of the electron density reflects the polarization of the Sr^{2+} electronic cloud towards the O^{2-} ions.

Atomic probability distribution functions

The refined Gram–Charlier anharmonic atomic displacement parameters at 296 and 145 K, calculated using atomic and ionic scattering factors, were used to calculate the atomic PDF's. Both models gave similar PDF's at

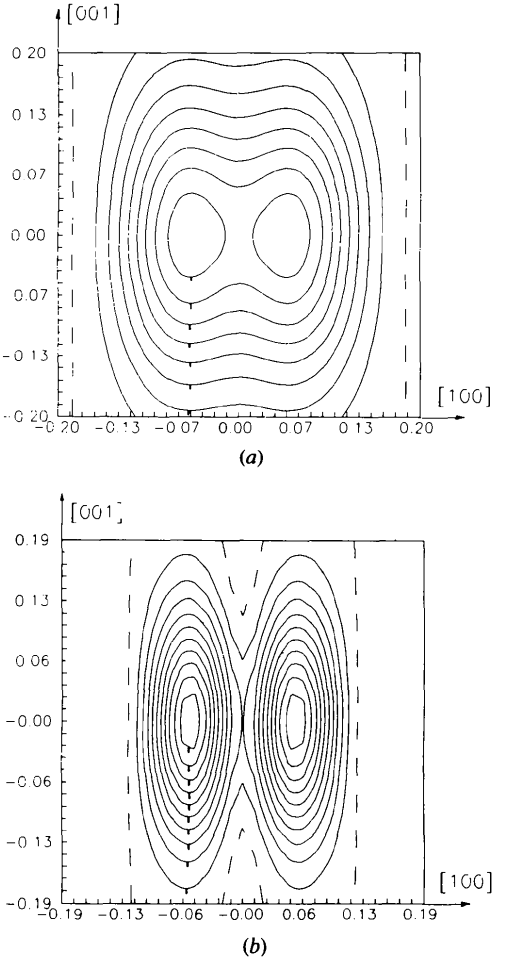

Fig. 3. Maps of anharmonic PDF's for the O atom in $SrTiO_3$ in the (100) plane: (*a*) 296 and (*b*) 145 K. The ideal crystallographic position of the atom in the unit cell ($\frac{1}{2}$, 0, 0) corresponds to the (0,0) coordinate on the maps. The Ti—O bond is horizontal. The distances in Å are shown along coordinate axes. Contour intervals are (*a*) 400 and (*b*) 1000 Å^{-3}. Positive, zero and negative contours are represented by solid, long and short dashed lines, respectively. The directions of the PDF decrease are shown by dashes perpendicular to the isolines.

both temperatures. However, the PDF's of the O^{2-} ion at 145 K and the Ti^{4+} ion at 145 and 296 K have physically meaningless regions with significant negative values at the site of the atoms when the ionic scattering factors were used. That is why only the PDF's obtained from the refinement using the atomic scattering factors will be discussed below. They are shown in Figs. 3, 4 and 5 for O, Ti and Sr atoms, respectively. A small region of negative PDF still remains at the Ti-atom site at 296 K (Fig. 4*a*). The appearance of such regions might be a consequence of the neglect of higher-order terms in the anharmonic expansion. However, the refinement using both ionic and atomic scattering factors with anharmonic terms up to six rank did not lead to significant higher-order terms.

The atomic PDF's of the O atom at $(\frac{1}{2}00)$ at both temperatures (Fig. 3) correspond to a highly anharmonic displacement distribution with two peaks on the line of the Ti—O bonds lying ±0.06 and 0.05 Å from the ideal position at 145 and 296 K, respectively. Between 296 and 145 K, the anisotropy of each of these peaks increases as a result of a strong decrease in the width of the peak along the Ti—O bond direction from 0.06 (half width at half maximum) to 0.03 Å. The width of the peak in the direction perpendicular to the bond changes only from 0.13 to 0.10 Å. Thus, the amplitude of the libration remains relatively constant. The PDF of the Ti atom (Fig. 4) is also strongly anharmonic, having the form of a spherical shell of thickness 0.05 and radius 0.10 Å at room temperature decreasing to 0.07 Å at 145 K. At the lower temperature the shell of Ti shows local maxima in the [110] and [111] directions. A similar form of the Ti atom PDF was noted by Palmer (1993) at 293 K, but was attributed to experimental error in the γ-ray diffraction measurement. The PDF around the Sr atom (Fig. 5) is essentially harmonic at room temperature, but at 145 K it too becomes strongly anharmonic, having the form of a flat-topped plateau of radius 0.06 Å.

The size instability that gives rise to the rotational phase transition makes no contribution to the anharmo-

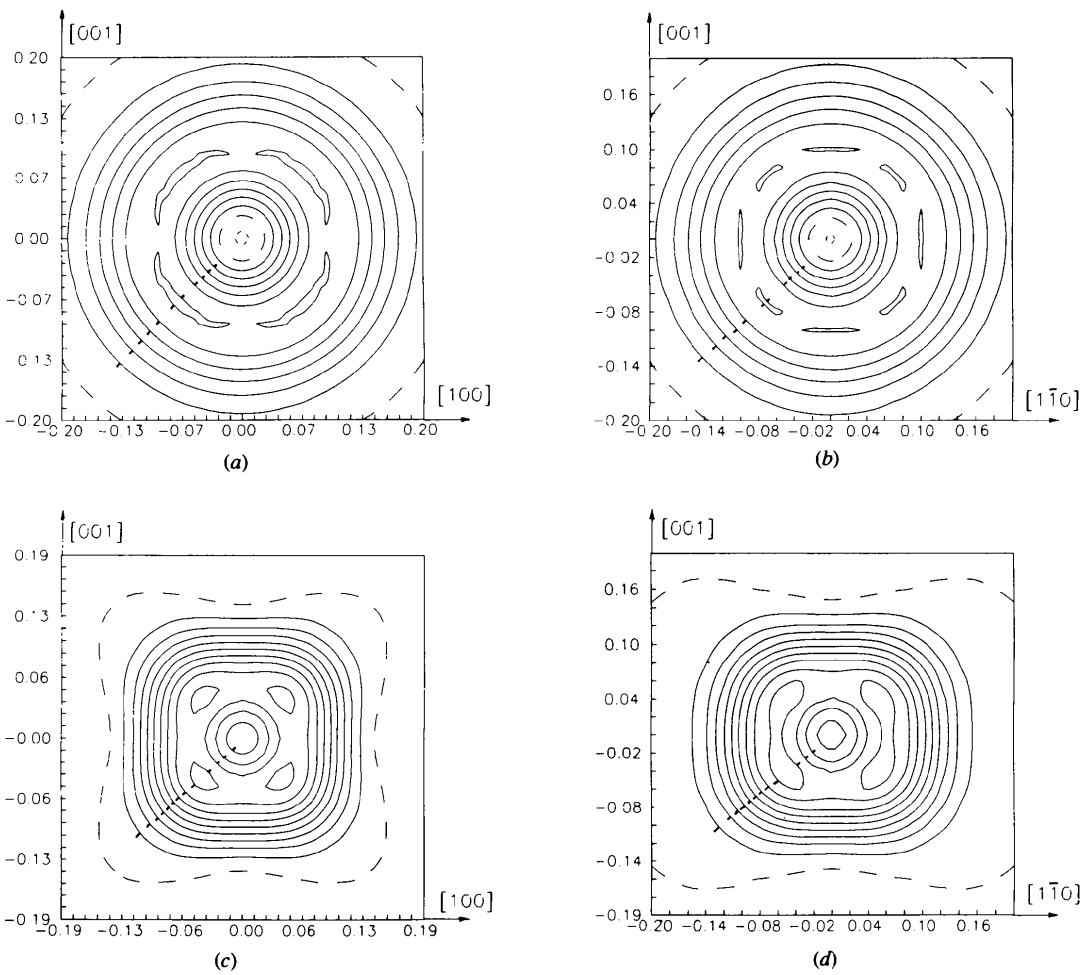

Fig. 4. Maps of the Ti-atom PDF in $SrTiO_3$: (*a*) 296 K, (100) plane; (*b*) 296 K, (110) plane; (*c*) 145 K, (100) plane; (*d*) 145 K, (110) plane. Contour intervals are 600 (*a*,*b*) and 1000 (*c*,*d*) $Å^{-3}$.

nicity of the Sr and Ti atoms, since these atoms are not displaced by a rotational phase transition. The only change expected is the displacement of the O atom perpendicular to the Ti—O bond. As mentioned above, such a displacement is suggested by the near constancy of the half width of the O peak in this direction. The rotational phase transition cannot account for the other features of the PDF's, namely the splitting of the O atom along the Ti—O bond direction, the spherical shell observed around Ti at both temperatures and the flat-topped plateau observed around Sr at the lower temperature.

In order to understand these results, it is helpful to consider first the instability of an atom moving in a one-dimensional anharmonic potential well. When an atom is placed at the center of symmetry, only even-powered anharmonic terms are present. These have the effects of flattening the potential near the minimum, while still allowing the potential to rise to large values at finite displacements. Increasing the anharmonicity leads to the appearance of two subsidiary minima equally placed on either side of the ideal position. As a result, the ideal position becomes a potential maximum. As long as this maximum is not more than kT above the minimum, the atom will be able to move easily from one minimum to the other but will spend more time near the minima and less time at the ideal position. If the anharmonicity increases further, the atom will be unable to cross the barrier and will remain locked into one minimum. At the point where the atom spends enough time in one minimum for the remaining structure to relax, the potential will become asymmetric, since the occupied minimum will relax to a lower energy than the unoccupied one. When this happens, the local site symmetry of the atom is reduced and the crystal will have gone through a phase transition.

The same behavior is found in three-dimensions, but the displacive behavior is more complex. Depending on the atomic site symmetry in the high-symmetry phase, several subsidiary minima will occur equidistant from the ideal position, either lying on the circumference of a circle (for the O atoms in perovskite) or the surface of a sphere (for the A and B atoms). The mechanism of reorientation between these minima will involve motion around the circle or sphere rather than through the ideal position, since the potential barriers on this surface will be lower than the potential barrier at the center. Thus, for a high enough degree of anharmonicity, the atom may move around the circle or sphere without ever crossing the ideal position. Even in this extreme, the crystal will retain its higher symmetry. The crystal symmetry will only be lowered when the atom remains in one minimum long enough for the surrounding structure to relax. This relaxation will, in turn, alter the potential minima in adjacent unit cells, resulting in a cooperative freezing out of the low-symmetry structure.

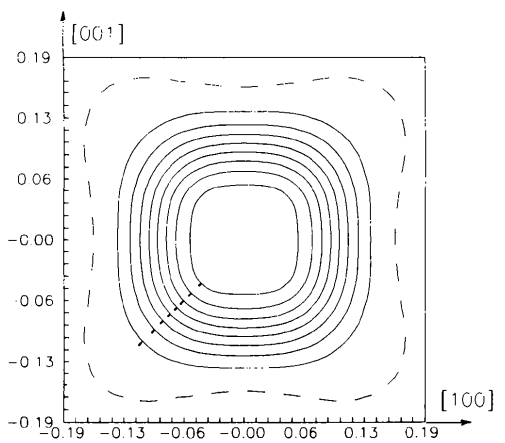

Fig. 5. Map of Sr-atom PDF in $SrTiO_3$ at 145 K in (200) plane. Contour interval is 1000 Å^{-3}.

Before application of these ideas to the cubic phase of $SrTiO_3$ we should note that the fourth-rank anharmonic parameters of the O atom show almost no variation with temperature. It may be due to the undescribed bonding features of the O atom or to static disorder of both. However, we suppose that the electronic contribution to fourth-rank displacement parameters is negligible because high-order refinement was used.

We expect that the librational motion of the TiO_6 octahedra (rotational distortion) will cause the atomic PDF of O to have a maximum lying on a circle centered at the ideal position and oriented perpendicular to the Ti—O bond. If the Ti atom displays a second-order Jahn–Teller distortion (displacive distortion), the cubic symmetry of $SrTiO_3$ would result in the atomic PDF of Ti having a maximum on the surface of a sphere with a minimum at the ideal position at its center. Contrary to the expectation that only one or the other distortion can occur depending on whether the tolerance factor is smaller than or greater than 1.0, the PDF's show that both types of distortion are present. We have found the maximum in the PDF of Ti at a distance 0.07–0.10 Å from the ideal position, suggesting that the Ti atom does undergo the second-order Jahn–Teller distortion. At room temperature, all possible displacements occur with equal probability, but at 145 K displacement towards an octahedral edge or face is favored over displacement towards a corner (Figs. 4*c* and *d*).

This distortion can be modeled using the weighted form of equation (2)

$$\sum_{\text{loop}}\{s_{ij}/W_{ij}\} = 0. \qquad (5)$$

Kunz & Brown (1995) have shown that the bond lengths found in the TiO_6 octahedra that show second-order Jahn–Teller distortions can be correctly reproduced by setting W to 1.3 for the two Ti—O bonds which are expected to be shortened and 0.7 for the two bonds *trans* to these. Solving (1) and (5) gives two short Ti—O

bonds of length 1.87 Å, two unchanged bonds of 1.96 Å and two lengthened bonds *trans* to the short bonds of 2.10 Å. The difference between the longest and shortest bonds is 0.23 Å. If one interprets the low-temperature atomic PDF's as indicating that the Ti and O atoms move towards each other, O by 0.06 Å and Ti (towards an octahedral edge) by 0.07 Å, a similar environment is produced in which the difference between the longest and shortest bond is 0.22 Å, in excellent agreement with the model. We therefore propose that the electronic instability arising from the overlap of the 3*d*-orbitals of Ti with the 2*p*-orbitals of O, which is observed on the deformation electron-density maps (Figs. 1 and 2), results in a displacement of Ti and O atoms towards (or away from) each other in such a way that some Ti—O bonds are shortened by 0.09 Å and the bonds *trans* to these are lengthened by 0.14 Å. The net effect of the distortion is to increase the average length of the Ti—O bonds by *ca* 0.02 Å, just enough to shift the tolerance factor in favor of a rotational phase transition.

The displacement of the O atom towards one Ti and away from the other ensures that the displacements of adjacent Ti atoms are correlated. In $BaTiO_3$ these correlations lead to long-range order and the freezing out of a ferroelectric phase, but this clearly does not happen in $SrTiO_3$, except possibly at the lowest temperatures, but short-range order must be present. The rotational displacements of the TiO_6 octahedra must also be correlated, since if one octahedron rotates clockwise, the neighboring ones must rotate anticlockwise. In the cubic phase both distortions will therefore show short-range order. If the rotational distortions were confined to a plane, *e.g.* all the octahedra rotate only about the *c* axis, they would have to show long-range order, since alternate octahedra must rotate in opposite directions in the manner of a chessboard. However, the displacive distortion of the Ti atom is only required to have long-range order if the displacement is confined to a single dimension. The rotational distortion therefore is intrinsically more likely to give rise to long-range order than the displacive distortion, accounting for the rotation freezing out at the higher temperature.

The rotational distortion does not result in the displacement of Sr from its ideal location, but a displacive distortion of Ti does. However, such a displacement will only appear in the cubic phase if the Ti atom stays in one position long enough for Sr to relax. The appearance of an anharmonic displacement of the Sr atom at 145 K indicates that the frequency of the reorientation of Ti is lowered as the temperature is reduced.

The picture of $SrTiO_3$ that emerges from the atomic PDF's is that of a crystal in which Ti shows a largely temperature-independent electronic distortion of the type often displayed by octahedrally coordinated Ti^{4+} ions. The effect of this distortion is to displace both the Ti and O atoms from their ideal positions. Although the positions of atoms in adjacent octahedra will be correlated, leading to short-range order, long-range order does not develop at the temperature studied, but at 145 K the motion of the Ti atoms is sufficiently slow that the Sr atoms have time to relax from their ideal positions. At room temperature the TiO_6 octahedra undergo a librational motion which does not decrease as the temperature is lowered. The librations show only short-range order above 106 K, the temperature at which long-range order appears. It would be interesting to know what happens below the 106 K transition where the rotational distortions have developed long-range order and frozen out, but where the displacive distortions presumably still show only short-range order.

The appearance of both incipient rotational and displacive distortions is surprising in a crystal with a tolerance factor of 1.00, where neither effect is expected if only geometry considerations are taken into account. The displacive transition is not, however, driven by the mismatch between the relative sizes of the Sr^{2+} and Ti^{4+} ions, which is what the tolerance factor measures, but by the electronic instability of Ti^{4+}. The resultant distortion of the TiO_6 octahedron causes the average Ti—O bond length to increase by 0.02 Å, just sufficient to reduce the tolerance factor to the point where a dynamic rotational distortion appears.

It is interesting to note that the PDF's of Ti and O atoms in $SrTiO_3$ resemble those in rutile TiO_2 (Restori, Schwarzenbach & Schneider, 1987). The TiO_6 bonding geometry is different, but the observations made for TiO_2 are in agreement with our results.

Summary

High-precision X-ray diffraction data at 296 and 145 K and the bond valence model calculation support the idea that cubic $SrTiO_3$ is subject to two types of instability: an electronic instability related to the Ti—O bonding and a size instability related to a small misfit between the Ti and Sr atoms in the ideal perovskite structure. At the temperatures studied, the anharmonic atomic probability functions show that these instabilities lead to two types of distortion with short-range order. The Ti atom lies dynamically off-center in the octahedron of its ligand O atoms, and the octahedra themselves librate, both effects showing signs of freezing out as the temperature is lowered. The electron-density distribution corresponds to ionic bonding for the Sr—O bonds, but the Ti—O bonds show concentrations of electron density that indicate an important contribution from covalent sigma bonding in agreement with calculated electron densities and the observed second-order Jahn–Teller effect.

VGT, VEZ and YAA wish to thank The Netherlands Organization for Scientific Research (NWO) for financial support of this work. The work was carried out in part with the aid of a research grant to IDB from the Natural

Science and Engineering Research Council of Canada. We are also thankful to anonymous referees for valuable comments.

References

ABRAHAMS, S. C. & KEVE, E. T. (1971). *Acta Cryst.* A**27**, 157–165.

BECKER, P. & COPPENS, P. (1974). *Acta Cryst.* A**30**, 129–147.

BILZ, H., BUETTNER, H., BUSSMANN-HOLDER, A. & VOGL, P. (1987). *Ferroelectrics*, **73**, 493–500.

BROWN, I. D. (1991). *Chemistry of Electronic Ceramic Materials*, edited by P. K. DAVIES & R. S. ROTH, NIST sp. pub. 804, pp. 471–483. Washington US Department of Commerce.

BROWN, I. D. (1992). *Acta Cryst.* B**48**, 553–572.

BROWN, I. D. & ALTERMATT, D. (1985). *Acta Cryst.* B**41**, 244–247.

BRUCE, A. D. & COWLEY, R. A. (1981). *Structural Phase Transitions*. London: Taylor and Francis Ltd.

BURDETT, J. K. (1980). *Molecular Shapes*. New York: John Wiley Interscience.

BUTTNER, R. H. & MASLEN, E. N. (1992). *Acta Cryst.* B**48**, 639–644.

COHEN, R. E. & KRAKAUER, H. (1990). *Phys. Rev.* B**42**, 6416–6423.

GLAZER, A. M. (1972). *Acta Cryst.* B**28**, 3384–3392.

HIRSHFELD, F. L. (1977). *Theor. Chim. Acta*, **44**, 129–138.

HOVESTREYDT, E. (1983). *Acta Cryst.* A**39**, 268–269.

HUTTON, J. & NELMES, R. J. (1981). *J. Phys. C*, **14**, 1713–1736.

IVANOV, I. V., BELOKOPYTOV, G. V., BUZIN, I. M., SYCHEV, V. M. & CHUPRAKOV, V. F. (1978). *Ferroelectrics*, **21**, 405–407.

KUNZ, M. & BROWN, I. D. (1995). To be published.

LYTLE, F. W. (1964). *J. Appl. Cryst.* **35**, 2212–2215.

LOBANOV, N. N., TSIRELSON, V. G. & SHCHEDRIN, B. M. (1990). *Sov. Phys. Crystallogr.* **35**, 344–347.

MEGAW, H. D. (1952). *Acta Cryst.* **5**, 739–749.

PALMER, A. (1993). PhD Thesis: Hahn–Meithner Institute, Berlin.

RESTORI, R., SCHWARZENBACH, D. & SCHNEIDER, J. R. (1987). *Acta Cryst.* B**43**, 251–257.

STIRLING, W. G. (1972). *J. Phys. C*, **5**, 2711–2730.

STRELTSOV, V. A. & ZAVODNIK, V. E. (1989). *Sov. Phys. Crystallogr.* **34**, 824–828.

TAKAZAWA, H., OHBA, S. & SAITO, Y. (1988). *Acta Cryst.* B**44**, 580–583.

UNOKI, H. & SAKUDO, T. (1967). *J. Phys. Soc. Jpn*, **23**, 546–552.

WEYRICH, K. H. & MADENACH, R. P. (1990). *Ferroelectrics*, **111**, 9–14.

WEYRICH, K.-H. & SIEMS, R. (1985). *Z. Phys. B*, **61**, 63–68.

XU, Y.-N., CHING, W. Y. & FRENCH, R. H. (1990). *Ferroelectrics*, **111**, 23–32.

ZACHARIASEN, W. F. (1967). *Acta Cryst.* A**23**, 558–564.

ZAVODNIK, V. E., STASH, A. I., TSIRELSON, V. G. & FEIL, D. (1994). XI Sagamore Conference on Charge, Spin and Momentum Densities. Abstracts, Brest, p. 259.

ZUCKER, U. H., PERENTHALER, E., KUHS, W. F., BACHMAN, R. & SCHULZ, H. (1983). *J. Appl. Cryst.* **16**, 358.